Correlative Fluorescence and Electron Microscopy of Whole Breast Cancer Cells Reveals Differential Distribution of ErbB2 Dependent on Underlying Actin

Indra Navina Dahmke[1], Patrick Trampert[2], Zahra Mostajeran[1], Franziska Lautenschläger[1,3] and Niels de Jonge[1,3]

[1]INM – Leibniz Institute for New Materials, Saarbrücken, Germany

[2]German Research Center for Artificial Intelligence, Saarbrücken, Germany

[3]Department of Physics, Saarland University, Saarbrücken, Germany

Abstract

Epidermal growth factor receptor 2 (ErbB2) is found overexpressed in many cancers such as gastric or breast cancer and is an important therapeutic target. ErbB2 plays a central role in cancer cell invasiveness and is, as such, closely linked to cytoskeletal reorganization. In order to study the spatial correlation of single ErbB2 proteins and actin filaments, we applied correlative fluorescence microscopy (FM), and scanning transmission electron microscopy (STEM) on specifically labeled SKBR3 breast cancer cells. For this purpose, the breast cancer cells were grown on microchips, transformed to express an actin-GFP fusion protein, and labeled with quantum dot (QD) nanoparticles attached to specific anti-ErbB2 Affibodies. FM was performed to identify the distribution of actin. For STEM of the intact plasma membrane of whole cells, the cells were fixed, and covered with graphene. Spatial distribution patterns of ErbB2 in the peripheral membrane regions were examined at actin-rich structures, and compared to adjacent actin-low regions of the same cell, revealing an association of ErbB2 homodimers with actin-rich regions. ErbB2 homodimers were found absent from actin-low membrane regions, and also after treatment of cells with Cytochalasin D. In both data sets, a significant inter-label distance of 36 nm was identified possibly indicating an association with

helical actin filaments. This finding was confirmed by identifying linear QD-chains in actin rich which showed an inter-label distance of 36 nm. In conclusion, single molecule analysis of whole cancer cells by means of STEM revealed different distribution patterns of membrane ErbB2 in dependency of the content of underlying actin filaments.

Introduction

The receptor tyrosine kinase ErbB2/Neu/HER2 forms together with ErbB1/EGFR/HER1, ErbB3/HER3 and ErbB4/HER4 the epidermal growth factor receptor (EGFR, ErbB) family. ErbBs play a role in cancer cell spreading and resemble important targets for cancer treatment.[1-3] ErbB2 can homo- or heterodimerize to induce a signaling cascade in cells leading to cell growth, motility and enhanced cell survival. Genetic amplification of ErbB2 was detected in different cancer types such as breast (25%) or ovarian cancer (30%).[4, 5] Patients with ErbB2 amplification show a poor prognosis due to the high rate of metastasis,[6] and, enhanced ErbB2 signaling was shown to induce motility and a metastatic phenotype in cancer cells, especially by formation of heterodimers with EGFR or ErbB3.[7-9] Overexpression of ErbB2 growth factor receptor strongly affects the actin cytoskeleton, and thus plays a role in the metastatic progression in cancer cells,[10, 11] which resembles indeed the major cause of mortality.[12] The interaction of ErbB2 with actin was reported previously in several studies, for instance, activated, heterodimerized ErbB2 was found to be associated with actin-rich membrane protrusions, like peripheral ruffles or filopodia-like protrusions, in ErbB2 overexpressing cells.[7-9, 13-15] Also, several other multi-protein-complexes have been shown to facilitate the direct interaction of ErbB2 with actin filaments,[9, 13, 15] such as binding via protein complexes including ezrin or actinin.[15, 16] A former study applying single-molecule detection in whole cells revealed the association of ErbB2 homodimers with membrane ruffles but did not assess the actin content of those.[17] Others showed that overexpression of either EGFR or

ErbB2 can lead to formation of membrane protrusions in cancer cells, which do not contain actin.[18, 19]

In order to gain further information on the interplay of ErbB2 and the actin cytoskeleton, we focused on specialized cell structures known as peripheral membrane ruffles, which show a high content of actin filaments. Membrane ruffles are also characterized by the high content of actin cross-linking proteins such as filamin and ezrin.[20] Peripheral membrane ruffles are furthermore described to be associated with ErbB2 proteins and closely linked to cancer cell motility.[8, 17, 21] In preceding work ErbB2 homodimers were found associated with membrane ruffles ,which are known to be centers of actin reorganization**.** In this report we study the spatial relation between ErbB2 distribution and cytoskeletal actin filaments. However, the combined analysis of membrane proteins on the single-molecule level in relation to the underlying cellular structure remains challenging. Electron microscopy (EM) provides the necessary spatial resolution, but in the course of conventional sample preparation, information about the related cellular structures has to be carefully reconstructed.[22] In our approach, we applied fluorescence microscopy and liquid phase scanning transmission EM (STEM) of whole cancer cells that were grown on silicon microchips and covered with graphene films and aim for the quantification of single molecules to test the effect of varying actin content on the distribution of ErbB2.

Materials and Methods

Cell culturing and labeling of Actin in SKBR3 breast cancer cells. Details of the protocol are described elsewhere [17, 23]. Human breast cancer SKBR3 cells (ATCC® LGC Standards GmbH, Germany, HTB-30™) were cultured in 25 cm² cell culture flasks (Greiner Bio-One GmbH, Germany, Cellstar®, TC™) with Dulbecco's Modified Eagle's Medium GlutaMAX™ (high glucose and pyruvate, DMEM, Gibco, ThermoFisher Scientific, USA)

containing 1% non-essential amino acids and 10% heat inactivated Fetal Bovine Serum (FBS, Gibco, ThermoFisher Scientific) under standard cell culturing conditions (at 37°C and 5% CO_2). SKBR3 cells serve as a common model system for ErbB2-overexpressing breast cancer.[2]

For correlative fluorescence and electron microscopy, cells were seeded two days prior to imaging on custom-made SiN-microchips (dimensions: $2.0 \times 2.6 \times 0.3$ mm^3, SiN-window: 0.50×0.15 mm^2 of 50 nm thickness, DensSolutions, The Netherlands). [24] In preparation, the microchips were cleaned with ArO_2-plasma for 5 minutes, then coated with poly-L-lysine (0.01%, Sigma-Aldrich, Germany) for 5 minutes at room temperature and washed twice with phosphate buffered solution (1×, pH 7.4, Gibco, ThermoFisher Scientific). The microchips were then coated with fibronectin (15 µg/mL, Sigma-Aldrich) under the same conditions. Immediately after, the microchips were transferred to a 96-well-plate (Greiner Bio-One GmbH, Cellstar®) and covered with 100 µL of FBS-free DMEM each. Next, SKBR3 cells were harvested with CellStripper (Corning, USA) and diluted to 200,000 cells per mL with 100 µL of the prepared cell-suspension added to each well. After 2-3 hours of incubation under standard culture conditions, the microchips were transferred to new wells pre-filled with 200µL of DMEM with CellLight™ Actin-GFP, BacMam 2.0 (30 particles per cell, Invitrogen, ThermoFisher Scientific) to transduce the cells with actin-GFP. The samples were cultivated for 40hrs and either treated with an actin-inhibitor (see below) for 1h or immediately labeled with anti-ErbB2 affibodies.

Labeling of ErbB2. For the labeling of ErbB2 molecules with quantum dots (QDs), microchips were rinsed once in GS-BSA-PBS (1% goat-serum (GS), Gibco; 1% BSA (molecular biology-grade albumin fraction V, Carl Roth GmbH-Co. KG, Germany); in PBS and incubated in the same solution for 5 minutes at 37°C for blocking unspecific binding sites before incubation with the biotin-conjugated anti-ErbB2-Affibodies® ((ZERBB2:477)2,

ErbB2-AFF-B, Affibody, Sweden). Next, microchips were incubated for 10 minutes at 37°C with 200 nM ErbB2-AFF-B in GS-BSA-PBS. After consecutive washing with 1%-BSA-PBS (2×), PBS(1×) and with cacodylate-buffer (1×, CB, 0.1 M sodium cacodylate trihydrate, Carl Roth GmbH, Germany, and 0.1 M saccharose, pH 7.4), the cells were fixed for 15 minutes at room temperature with 4% formaldehyde (Electron Microscopy Sciences, USA) in CB to prevent QD-induced clustering of ErbB2-molecules. Next, cells were rinsed once with CB and three times with PBS-BSA, and then incubated in 0.1 M glycine in PBS for 2 minutes. After two additional washes with PBS, cells were incubated with streptavidin-conjugated Qdot 655 (5 nM, Life Technologies, USA) in borate buffer (40 mM, sodium tretraborate boric acid, Sigma-Aldrich, pH 8.3) at room temperature for 12 minutes. Finally, cells were washed three times in PBS-BSA (1%) and subjected to fluorescence imaging. Further practical details of the protocol including meticulous control experiments for unspecific binding of QDs are reported elsewhere.[23]

After fluorescence imaging of the samples, an additional fixation step was added to enhance the stability of the cellular structures for imaging by means of EM. The cells where fixed with 2% glutaraldehyde in CB buffer for 12 min and rinsed once with CB and three times with PBS-BSA. Samples were stored in PBS-BSA at 4°C until covering with graphene was conducted.

Disruption of actin containing ruffles. Cytochalasin D (Sigma-Aldrich) was applied to SKBR3 cells to disrupt the formation of peripheral ruffles by disturbance of the actin network. For this purpose, the cells were transduced with actin-GFP and seeded on Si microchips as described above. After 40 hours of cultivation, cells were examined by light microscopy prior to incubation with either DMSO (negative control, Carl Roth GmbH-Co. KG, Germany) or 2 µM of Cytochalasin D in GS-BSA-PBS for 60 minutes at 37°C and 5% CO_2. This concentration was applied before to SKBR3 cells[25] and shown to inhibit membrane ruffling

after 10 min.[26] Incubation with the anti-ErbB2-Affibody for 10 minutes at 37°C and 5% CO_2 followed and a staining procedure was performed as described above.

Light microscopy. After fixation with formaldehyde, the samples were imaged with an inverted light microscope (DMI 6000B, Leica, Germany). For this purpose, the microchips were placed upside-down in a plasma-cleaned cell culture dish with a glass bottom (35 mm in diameter, MatTek Coperation, USA) filled with PBS-BSA (1%) and imaged with 20× (HCX PL Fluo TAR L, 0.40, dry, Leica), 40× (HCX PL Fluo TAR L, 0.60, dry, Leica) , or 63x oil (HC PL APO 63x/1.40 oil) objectives in direct interference contrast (DIC) and fluorescence mode (filter cube L5: excitation: 460-500 nm, DIM: 505 nm, emission: 512-542 nm and TX2: excitation: 540-580 nm, DIM: 595 nm, emission: 607-683). Cellular regions expressing high levels of ErbB2 or EGFR emitted a red fluorescence (at λ=655 nm), whereas actin fibers emitted green fluorescence (at λ=520 nm). The images were acquired by employing the LAS FX operational software (Leica) and for overview images manually stitched together.

Graphene deposition. Polymethylmethacrylat (PMMA) covered graphene ("trivial transfer graphene", ACS Materials, USA) was removed from its polymer support according to instructions of the manufacturer and left overnight in a 10% sodium persulfate solution to remove potential copper contaminants from the production process, which interfere with protein labeling for STEM. Afterwards, the graphene film was washed in deionized H_2O three times, transferred to a salt crystal (International crystal laboratory, USA), and baked for 20 minutes at 100°C. Finally, the PMMA was removed from the graphene film by incubating the graphene-salt for 30 minutes in acetone (100%, high pressure liquid chromatography grade, Carl Roth GmbH-Co. KG) at 30°C. This step was repeated two times. To transfer the graphene film onto cancer cells grown on microchips, the graphene-NaCl crystals were placed on the surface of pure H_2O (Carl Roth GmbH-Co. KG) as described elsewhere. [27, 28] Once the underlying NaCl was dissolved completely, the free-floating graphene film was lifted out with

the microchip using a pair of forceps. The position of the graphene film over the SiN-window was then verified with a binocular and carefully corrected with forceps if necessary. The microchip was left to air dry at room temperature for about 5 minutes, and then stored in a humid chamber at 4°C until imaging.

STEM. STEM images were acquired with a transmission electron microscope (JEM-ARM 200F, JEOL, Japan) equipped with a cold field emission gun and a STEM probe corrector (CEOS GmbH, Germany). The microchip was mounted on a standard TEM sample holder (JEOL) and the sample was imaged with an electron beam of 200 keV. In STEM mode, images were recorded with a pixel dwell time of τ = 14 µs. The electron probe setting was 4c combined with an aperture CL2-3 with 20 µm diameter, resulting in a probe current of I_p = 63 pA, and an electron dose of 67 $e^-/Å^2$ for a magnification of 100,000× (the pixel size was 1 nm with 2,048 x 2,048 image resolution). The camera length was set to 8 cm, leading to a detector opening semi-angle of 43 mrad for the angular dark field detector. This relates to the opening through which electrons pass the detector, although, the actual collection angle is larger.

QD-label analysis. For the detection of QD-labeled ErbB2 membrane proteins in the STEM micrographs, we applied an automated analysis,[17] which was programmed in ImageJ (National Institute of Health, USA). STEM images were preprocessed by checking for contaminating electron dense particles different from QDs that is of a larger size to avoid false counting of label positions. In case contaminating particles were present, STEM micrographs were altered by manually greying out the latter contaminations. The images were further processed automatically. A Gaussian filter was first applied with a radius of 1.5 pixel for noise-filtering. Variations in the image background were then filtered using a Fourier filter. The image was subsequently binarized by applying an automated threshold with maximal entropy settings. The program accounted for a bin width set to 2 nm and particles with a size

> 10 nm. For the subsequent statistical analysis by a pair correlation function g(r), a locally designed software tool in C++ was used[17]. The pair correlation function was defined as: [29]

$$g(r) = \frac{1}{\pi\rho^2 r\gamma(r)} + \sum_{i=1}^{N} \sum_{j=i+1}^{N} k\left(\mathrm{r} - \left|x_i - x_j\right|\right) \qquad (1)$$

with r the radial distance, and ρ the labeling density in the image. The covariance function, $\gamma(r)$, and the kernel, k, are defined elsewhere [30]. The modulus $\left|x_i - x_j\right|$characterizes the distance between two reference points, i and j, with x indicating for the two-dimensional coordinates (x, y) of a particles in the analyzed micrograph. This calculation of g(r) assumes a planar location of the QD-labeled membrane proteins. The QD-label distribution was analyzed for different experimental groups by adding all label positions acquired in all images of that group.

In order to test the significance of the results of the statistical analysis by the pair correlation function, we applied an in-house programmed imageJ plug-in to generate data sets with a random particle distribution but a definable particle density. So for the comparison of the experimental data derived from the STEM images, we generated the same number of random images as in the respective experimental data set, containing the average QD-particle density of this set. The generated random data was then prospected to pair correlation analysis in the same way as the experimental data sets.

QD-particle chain analysis. Linear QD-particle chains were automatically searched in the STEM images (=experimental datasets). As shown before,[31] it was experimentally demonstrated that six particles in order suffice, to build such a particle chain, which was experimentally validated by the help of a statistical analysis. We selected the same parameters as described before that means (i) the distance between consecutive particles on a line was

allowed to be 36±15 nm, and (ii) the angle of connecting lines between three particles in a row was allowed to be 180±30°. The experiments were conducted in Matlab (MATLAB and Statistics Toolbox Release 2018a. The MathWorks, Inc., Natick, Massachusetts, USA) using an in-house developed program.[31] The corresponding pseudo-code is illustrated in Scheme 1.

Additionally, we generated random particle data and evaluated these as well. Each investigated image was divided into 8×8 segments. The particle positions in each segment were then randomized. This procedure ensures that the large-scale structure i the image, for example localized protein densities, are preserved but discards the exact positioning. We run the algorithm on the randomized data and compared the results to the linear structures detected in the experimental data. These comparisons showed that our findings were not based on random effects as the source of our observations.

Results

Method for single-molecule microscopy of ErbB2 correlated to presence of actin. A correlative microscopy method was established to analyze the spatial correlation of the functional state of ErbB2 with the abundance of actin in whole cells (Fig. 1). SKBR3 breast cancer cells grown on silicon microchips, were first transduced with an actin-GFP baculovirus construct, and cultivated for 40h. Optionally, breast cancer cells were incubated with Cytochalasin D for 1h to induce de-polymerization of the actin cytoskeleton and disruption of membrane ruffles.[32] In the following steps, the breast cancer cells were incubated with a specific biotin-conjugated anti-ErbB2-Affibody, fixated with paraformaldehyde to prevent artificial clustering of labels, and marked with fluorescent, streptavidin-conjugated QDs. Cell regions of interest containing higher amounts of both actin and ErbB2 were then identified using light microscopy (Fig. 2).

To protect the hydrated samples from drying when being placed in vacuum during electron microscopy, each microchip was covered with a multi-layered graphene film, using a method to transfer graphene floating on a water surface onto the sample (Fig. 1).[27] The samples were then imaged with STEM, first at low magnification (1000-2000 ×) in order to correlate the cell locations in the images obtained by light microscopy with the ones obtained by means of electron microscopy (Fig. 2). Areas of interest identified via light microscopy were thus found back in the electron microscopy images, and were examined using STEM at higher magnification (100,000-120,000 ×) so that single labels were visible (Fig. 2e, f) from which the functional state of ErbB2 was determined as described in the following section.

Statistical method to determine functional state of ErbB2. In order to distinguish ErbB2 proteins forming homodimers from ones that were randomly grouped at closer vicinities, the label position data was statistically analyzed using the pair correlation function $g(r)$.[17, 30] The $g(r)$ gives the probability of finding two labels at a certain radial distance r with $g(r) = 1$ indicating for random positioning. An average center-to-center distance of 20 nm is expected between two QDs each attached to an ErbB2 protein in a homodimer.[17] But this value has some variation due to flexibility of the linkers. The functional state of ErbB2 is thus detected via labeling of single, endogenous ErbB2 proteins with a high abundancy in the cell membrane.[33] Such data is not obtained with other techniques using, for example, whole antibody complexes or artificial fusion proteins as labels.[34, 35] The subsequent statistical analysis corrects for false positive readings by excluding randomly paired labels, which might be the case with proximity techniques such as proximity ligation or fluorescence resonance energy transfer assays.[35, 36]

Distribution of membrane-bound ErbBs in relation to actin-GFP

In order to correlate the distribution of QD-labels with the occurrence of actin-GFP, we analyzed STEM images collected at two different membrane regions. For the first group,

STEM images were collected in cell areas that were identified by the presence of the fluorescence signal for actin-GFP, and peripheral membrane ruffles as identified in DIC mode as described elsewhere (Fig. S1).[17] Here, we found a higher density of QD-labels when compared to cell areas with a low content of actin (Table 1). The resulting graph of $g(r)$ collected at cell actin rich cell regions displayed a peak at 20 nm exceeding random level (Fig. 3a). This peak is significant above the statistical fluctuations, since $g(r) - 1 > 3*SD$, with SD the standard deviation of the $g(r)$ for 50 nm < r < 200 nm, beyond the peak, and the factor of 3 originating from the Rose criterion.[37] This plasma membrane area thus contained signaling-active homodimers.[1, 17] For comparison, a simulation of a random distribution of QD-labels of this size was included in Fig. 3a as well.

For the second group, STEM micrographs were collected in adjacent membrane regions with low signal for actin-GFP compared to the first group. In contrast to the $g(r)$ of actin-rich regions, the $g(r)$ of membrane areas with lower actin content showed no peak at 20 nm but at 36 nm (Fig. 3b). This graph also displays larger fluctuations due to the lower number of collected QD positions compared to the actin rich regions (Table 1). A similar level of fluctuations is visible in the corresponding random simulation of QD positions of the same density and amount (Fig. 3b). The peak at 36 nm is nevertheless significant since the SD = 0.10 of the $g(r)$ (for 50 nm < r < 200 nm). The presence of a 36-nm peak was possibly caused by a substantial fraction of ErbB2 interacting with overexpressed actin in the analyzed cells, since it was hypothesized previously that ErbB2 would bind in a chain-like orientation to actin[31] at intervals of ~36 nm.[38] To test if the peak was caused by a high expression level of actin, we performed a pair correlation analysis of QD-labels in flat membrane regions of cells that were negative for actin-GFP in the fluorescence images. In accordance with former findings, no peak at 36 nm was detected (Fig. S2).

A further observation is that $g(r) > 1$ for the largest range of r in all experiments. This observation possibly indicates clustering of groups of labels or curvature of the plasma membrane. [39]

Cytochalasin D induces changes on membrane ErbB2 distribution. Next, it was tested if the formation of ErbB2 homodimers at peripheral membrane ruffles depended on the underlying actin network. Therefore, we treated SKBR3 cells with 2 µM Cytochalasin D for 1 h in order to disturb membrane ruffling. Cytochalasin D is a fungal metabolite that binds to the barbed end of actin filaments and inhibits the association and dissociation of actin monomers.[40] This treatment causes a disruption of the actin network, and induces the formation of actin foci, cell rounding, and inhibition of peripheral ruffle formation.[26, 32] It can be observed in Fig. S3 that Cytochalasin D induces loss of membrane ruffling and cell rounding in SKBR3 cells. Furthermore, Cytochalasin D incubation induced the formation of distinct, fingerlike protrusions, known as dendrites,[41] which can be observed in the STEM image of CD treated cells (Fig. 4a, b). The surface density of QD-labels in these affected membrane regions was lower than measured in cell regions with high and low actin contents in untreated cells (Table 1). Subsequent statistical analysis of the QD-labeled ErbB2 proteins showed an ErbB2-pattern similar to that of flat areas in untreated cells where the peak at 20 nm was lost, but here a prominent peak at 32-36 nm was registered (Fig. 4c). These results confirm that the formation of ErbB2 homodimers is coupled to an intact actin network in the membrane of SKBR3 cells.

Detection of linear QD-chains in actin rich membrane regions. After the detection of the inter-label distance of 36 nm above random in certain experimental data sets, we conducted a search for linearly arranged QDs in the STEM images of all data sets, namely, actin-GFP rich, actin-GFP low and Cytochalasin D treated cells.[31] A linear particle chain was defined to consist of consecutive QDs with an inter-label distance of 36±15 nm, and an angle of three

consecutive QDs in a row of 180±30°. Linear chains were detected that complied with these parameters in 3 STEM images acquired in actin-GFP rich regions (Fig. 5) but not in the other datasets (Table 2). In order to test if the identified lines were due to false positive pattern-detection, random particle data were generated for the according particle densities. For each image 100 randomized data sets were generated, and the probability of finding at least the number of particle-chains that were detected in the according experimental data set was calculated. The calculated p-values were below 0.04 for all three data sets, indicating that the detected QD-particle chains did not form randomly. A fraction of ErbB2 thus adhered directly or indirectly with filaments of the actin cortex in actin-GFP rich region.

Discussion

In this study, we applied correlative fluorescence microscopy and STEM to study graphene-covered whole cancer cells in order to investigate distribution patterns of membrane ErbB2 in spatial relation to actin. Our approach facilitated the detection and quantification of endogenous ErbB2 membrane proteins with a high abundancy at the single molecule level. It allowed for the assessment of the functional state of ErbB2 proteins, as well as for the spatial correlation with underlying structures. This is advantageous compared to conventional light microscopy, flow cytometry or gel electrophoresis that offer lower spatial resolution or lack the possibility of spatial analysis altogether.[17] We also performed a subsequent statistical analysis of our data that corrects for false positive read-outs by excluding randomly paired proteins, which might account for artefacts in proximity assays such as proximity ligation or fluorescence resonance energy transfer assays.[35]

A higher density of ErbB2 proteins was observed in actin-GFP rich membrane areas of the cell, such as peripheral ruffles, compared to membrane areas with a low content of actin-GFP. This observation is in accordance with previous publications that described activated

ErbB2 to be associated with actin-rich membrane protrusions in ErbB2 overexpressing cells.[7-9, 13-15] The capability of our approach for single molecule detection enabled the additional finding of paired, QD-labeled ErbB2 proteins with an inter-label distance of 20 nm above random, thus accounting for homodimerization of ErbB2 in actin-GFP rich peripheral membrane regions such as ruffles. The signaling active ErbB2 homodimers are thus preferentially found in membrane regions with an abundance of underlying actin. Previously, ErbB2 homodimers were observed to reside preferentially in ruffled cellular regions,[17] from which the question arose as to whether the homodimer was in a direct or indirect way coupled to actin as a mechanism explaining its preferential location in these membrane areas. The new data now indicates that a spatial linkage between actin and ErbB2 exists.

One reason for the spatial correlation of ErbB2 homodimers with peripheral membrane ruffles could be that ruffles resemble specialized regions that are enriched not only with densely packed actin filaments but also with cholesterol,[42, 43] and lipid rafts.[44] In fact, depletion of cholesterol inhibits the formation of membrane ruffling[42] and cholesterol enrichment induces ruffling in adherent cells.[43] It was furthermore described that ErbB2 clusters within lipid rafts, leading to homodimerization.[45] This might be due to the higher freedom of lateral movement of ErbB2 in lipid rafts when compared to ErbB2 in the plasma membrane outside lipid rafts due to the higher cholesterol content within lipid rafts. The lateral movement of EGFR, on the other hand, is not alternated in a lipid raft because it is bound to actin.[46] Thus, a higher probability may exist for ErbB2 to form homodimers rather than forming heterodimers with EGFR in the membrane ruffles.

At peripheral membrane regions with a low content of actin-GFP, a peak at 20 nm was not present in the pair correlation function. Instead, a peak at 36 nm was observed. A protein distance of ~36 nm was formerly proposed to be caused by the association of ErbB2 with actin filaments.[31] This association is counter intuitive because, in contrast to EGFR, ErbB2

does not comprise an actin binding domain.[47] We suggest that the inter-label distance of 36 nm is due to formation of EGFR:ErbB2 heterodimers, and the binding of EGFR to cortical actin, that is actin just below the plasma membrane actin. Others measured inter-label distances of fluorophore labeled EGFR-affibody by fluorophore localization imaging with photo bleaching (FLIP), and measured a value of 37 nm, which is of a similar dimension as the repeat of the left-handed helix of cortical, filamentous actin of 35.9 nm.[38] The finding of a 36-nm peak in flat regions was confirmed in a control experiment in which the ruffles were destroyed via CD leading to a mostly flat-like membrane. However, the 36-nm peak was absent from data obtained for cells that were negative for actin-GFP in the fluorescence images (Fig. S2). It can thus be concluded that the hypothesized heterodimers become sufficiently abundant for observation only for cells with overexpressed and intact networks formed by actin-GFP.

We also analyzed the data in a second way by conducting a search for linear QD-chains in all data sets (Fig. 5). Here, an opposite result was found considering the 36-nm peak, QD-chains with in inter-label distance of 36 ± 15 nm were found now in actin-GFP rich membrane regions, and not in membrane areas with a low content of actin-GFP, consistent with previous findings for ruffled regions.[31] This finding of linear chains shows that the assumption of the presence of heterodimers would also apply for actin-rich regions, but for this region, the number of homodimers was presumably larger than the number of heterodimers to such an extent that the 36-nm peak was not visible in the pair correlation function. There might have been linear chains also in the flat regions but those remained unobserved probably due to the limited labeling efficiency, resulting in a reduced probability of detecting 6 or more particles in one line. The labeling efficiency is unknown but if we assume a high labeling efficiency of 70% then the probability to find a linear chain of 6 amounts to 0.7^6=12% only. So, there might just not have been sufficient QD-labels in the flat areas for detecting lines.

Thus, EGFR:ErbB2 heterodimers seem to reside both in- and outside actin-GFP rich regions. Downstream signaling upon EGFR:ErbB2 heterodimerization induces motility[8] and promotes invasion of cancer cells through an extracellular matrix[48]. In fact, Brandt et al.[8] found a co-localization of EGFR and ErbB2 at areas where the cancer cells showed changes in their shape. They attributed the cellular shape changes to activation by the EGFR:ErbB2 heterodimers via immediate transphosphorylation of the protein gelsolin that end-blocks actin filaments. This mechanism requires the spatial proximity of the signaling active dimer to actin and actin-bound proteins. In this regard, the distribution analysis on the single molecule level and the spatial correlation with actin filaments, which we are able to obtain with our approach, conveys also a direct relation between functional state of ErbB2 in relation to the presence of actin filaments via EGFR as a probable linker to actin.

Conclusion

By applying correlative light microscopy and STEM of single, QD-labeled ErbB2 proteins in actin-GFP transduced breast cancer cells it was possible to detect distinct distribution patterns of membrane ErbB2 in dependency of the underlying actin content. Signaling active ErbB2 homodimers were detected in membrane regions with densely packed actin filaments but not in regions without actin-GFP. The observation of a peak in the label pair distance of 36 nm suggests an interaction of ErbB2 with cortical actin filaments, most probably via heterodimerization with EGFR. With our approach we were able to show distinct distribution patterns of membrane ErbB2 that in dependency of the underlying actin content.

Acknowledgements

We thank Florian Weinberg for discussions, Sercan Keskin for preparation of salt crystal-supported graphene sheets, Peter Kunnas for support with electron microscopy, Stephanie Smolka and Tabea Trampert for technical support, Daniel Gaa for programming a random image generator as imageJ plugin, and E. Arzt for his support through INM. The research was funded by the DFG SFB1027, and the Else Kröner Fresenius Stiftung.

References

(1) Citri, A.; Yarden, Y. *Nat Rev Mol Cell Biol* **2006,** 7 (7), 505-16.

(2) Henjes, F.; Bender, C.; von der Heyde, S.; Braun, L.; Mannsperger, H. A.; Schmidt, C.; Wiemann, S.; Hasmann, M.; Aulmann, S.; Beissbarth, T.; Korf, U. *Oncogenesis* **2012,** 1, e16.

(3) Hynes, N. E.; MacDonald, G. *Curr Opin Cell Biol* **2009,** 21 (2), 177-84.

(4) Loibl, S.; Gianni, L. *Lancet* **2017,** 389 (10087), 2415-2429.

(5) Scholl, S.; Beuzeboc, P.; Pouillart, P. *Ann Oncol* **2001,** 12 Suppl 1, S81-7.

(6) Moasser, M. M. *Oncogene* **2007,** 26 (45), 6469-87.

(7) Benlimame, N.; He, Q.; Jie, S.; Xiao, D.; Xu, Y. J.; Loignon, M.; Schlaepfer, D. D.; Alaoui-Jamali, M. A. *J Cell Biol* **2005,** 171 (3), 505-16.

(8) Brandt, B. H.; Roetger, A.; Dittmar, T.; Nikolai, G.; Seeling, M.; Merschjann, A.; Nofer, J. R.; Dehmer-Moller, G.; Junker, R.; Assmann, G.; Zaenker, K. S. *FASEB J* **1999,** 13 (14), 1939-49.

(9) Jeong, J.; Kim, W.; Kim, L. K.; VanHouten, J.; Wysolmerski, J. J. *PLoS One* **2017,** 12 (4), e0174849.

(10) Brix, D. M.; Clemmensen, K. K.; Kallunki, T. *Cells* **2014,** 3 (1), 53-78.

(11) Day, K. C.; Lorenzatti Hiles, G.; Kozminsky, M.; Dawsey, S. J.; Paul, A.; Broses, L. J.; Shah, R.; Kunja, L. P.; Hall, C.; Palanisamy, N.; Daignault-Newton, S.; El-Sawy, L.; Wilson, S. J.; Chou, A.; Ignatoski, K. W.; Keller, E.; Thomas, D.; Nagrath, S.; Morgan, T.; Day, M. L. *Cancer Res* **2017,** 77 (1), 74-85.

(12) Weaver, A. M. *Clin Exp Metastasis* **2006,** 23 (2), 97-105.

(13) Jeong, J.; VanHouten, J. N.; Dann, P.; Kim, W.; Sullivan, C.; Yu, H.; Liotta, L.; Espina, V.; Stern, D. F.; Friedman, P. A.; Wysolmerski, J. J. *Proc. Natl. Acad. Sci.* **2016,** 113 (3), E282-90.

(14) Mori, S.; Akiyama, T.; Morishita, Y.; Shimizu, S.; Sakai, K.; Sudoh, K.; Toyoshima, K.; Yamamoto, T. *Virchows Arch B Cell Pathol Incl Mol Pathol* **1987,** 54 (1), 8-15.

(15) Wang, S. E.; Shin, I.; Wu, F. Y.; Friedman, D. B.; Arteaga, C. L. *Cancer Res* **2006,** 66 (19), 9591-600.

(16) Jeong, J.; Choi, J.; Kim, W.; Dann, P.; Takyar, F.; Gefter, J. V.; Friedman, P. A.; Wysolmerski, J. J. *J Biol Chem* **2019,** 294 (3), 887-901.

(17) Peckys, D. B.; Korf, U.; de Jonge, N. *Sci. Adv.* **2015,** 1 (6), e1500165.

(18) Chung, I.; Akita, R.; Vandlen, R.; Toomre, D.; Schlessinger, J.; Mellman, I. *Nature* **2010,** 464 (7289), 783-7.

(19) Chung, I.; Reichelt, M.; Shao, L.; Akita, R. W.; Koeppen, H.; Rangell, L.; Schaefer, G.; Mellman, I.; Sliwkowski, M. X. *Nat Commun* **2016,** 7, 12742.

(20) Borm, B.; Requardt, R. P.; Herzog, V.; Kirfel, G. *Exp Cell Res* **2005,** 302 (1), 83-95.

(21) Feldner, J. C.; Brandt, B. H. *Exp Cell Res* **2002,** 272 (2), 93-108.

(22) Wolf, S. G.; Houben, L.; Elbaum, M. *Nat Methods* **2014,** 11 (4), 423-8.

(23) Peckys, D. B.; de Jonge, N. *Journal of visualized experiments : JoVE* **2015,** 103, e53186.

(24) Ring, E. A.; Peckys, D. B.; Dukes, M. J.; Baudoin, J. P.; de Jonge, N. *J. Microsc.* **2011,** 243 (3), 273-83.

(25) Stofega, M. R.; Sanders, L. C.; Gardiner, E. M.; Bokoch, G. M. *Mol Biol Cell* **2004,** 15 (6), 2965-77.

(26) Yahara, I.; Harada, F.; Sekita, S.; Yoshihira, K.; Natori, S. *J Cell Biol* **1982,** 92 (1), 69-78.

(27) Dahmke, I. N.; Verch, A.; Hermannsdorfer, J.; Peckys, D. B.; Weatherup, R. S.; Hofmann, S.; de Jonge, N. *ACS nano* **2017,** 11 (11), 11108-11117.

(28) Textor, M.; de Jonge, N. *Nano Lett* **2018**.

(29) Stoyan, D.; Stoyan, H. *Biom. J.* **1996,** 38 (3), 259-271.

(30) Stoyan, D.; Bertram, U.; Wendrock, H. *Ann. Inst. Statist. Math.* **1993,** 45 (2), 211-221.

(31) Parker, K.; Trampert, P.; Tinnemann, V.; Peckys, D.; Dahmen, T.; de Jonge, N. *Biophys J* **2018,** 115 (3), 503-513.

(32) Schliwa, M. *J Cell Biol* **1982,** 92 (1), 79-91.

(33) Yang, S.; Raymond-Stintz, M. A.; Ying, W.; Zhang, J.; Lidke, D. S.; Steinberg, S. L.; Williams, L.; Oliver, J. M.; Wilson, B. S. *J Cell Sci* **2007,** 120 (Pt 16), 2763-73.

(34) Liu, P.; Sudhaharan, T.; Koh, R. M.; Hwang, L. C.; Ahmed, S.; Maruyama, I. N.; Wohland, T. *Biophys J* **2007,** 93 (2), 684-98.

(35) Needham, S. R.; Hirsch, M.; Rolfe, D. J.; Clarke, D. T.; Zanetti-Domingues, L. C.; Wareham, R.; Martin-Fernandez, M. L. *PLoS One* **2013,** 8 (5), e62331.

(36) Greenwood, C.; Ruff, D.; Kirvell, S.; Johnson, G.; Dhillon, H. S.; Bustin, S. A. *Biomol Detect Quantif* **2015,** 4, 10-6.

(37) Rose, A., *Vision: human and electronic*. Plenum Press: New York, 1973.

(38) Needham, S. R.; Zanetti-Domingues, L. C.; Hirsch, M.; Rolfe, D. J.; Tynan, C. J.; Roberts, S. K.; Martin-Fernandez, M. L.; Clarke, D. T. *Biochem Soc Trans* **2014,** 42 (1), 114-9.

(39) Peckys, D. B.; Hirsch, D.; Gaiser, T.; de Jonge, N. *Molecular medicine* **2019,** 25 (1), 42.

(40) Cooper, J. A. *J Cell Biol* **1987,** 105 (4), 1473-8.

(41) Ting-Beall, H. P.; Lee, A. S.; Hochmuth, R. M. *Ann Biomed Eng* **1995,** 23 (5), 666-71.

(42) Grimmer, S.; van Deurs, B.; Sandvig, K. *J Cell Sci* **2002,** 115 (Pt 14), 2953-62.

(43) Qin, C.; Nagao, T.; Grosheva, I.; Maxfield, F. R.; Pierini, L. M. *Arterioscler Thromb Vasc Biol* **2006,** 26 (2), 372-8.

(44) Balasubramanian, N.; Scott, D. W.; Castle, J. D.; Casanova, J. E.; Schwartz, M. A. *Nat Cell Biol* **2007,** 9 (12), 1381-91.

(45) Nagy, P.; Vereb, G.; Sebestyen, Z.; Horvath, G.; Lockett, S. J.; Damjanovich, S.; Park, J. W.; Jovin, T. M.; Szollosi, J. *J Cell Sci* **2002,** 115 (Pt 22), 4251-62.

(46) Orr, G.; Hu, D.; Ozcelik, S.; Opresko, L. K.; Wiley, H. S.; Colson, S. D. *Biophys J* **2005,** 89 (2), 1362-73.

(47) den Hartigh, J. C.; van Bergen en Henegouwen, P. M.; Verkleij, A. J.; Boonstra, J. *J Cell Biol* **1992,** 119 (2), 349-55.

(48) Zhan, L.; Xiang, B.; Muthuswamy, S. K. *Cancer Res* **2006,** 66 (10), 5201-8.

(49) Yen, J. Y. *Q Appl Math* **1970,** 27, 526-&.

(50) Fisher, R. A. *Metron* **1921,** 1, 3-32.

Tables

Experimental group	No. of cells	No. of images	No. of all particles	Total density (particles /nm²)	Total area (nm²)	Average particle density per image (particles/nm²)
Actin low	8	17	1,640	41*10^-5	7*10^7	2.4*10^-5
Actin rich	11	27	13,807	334*10^-5	11*10^7	12.4*10^-5
CD	5	7	400	11*10^-5	2.5*10^7	1.6*10^-5

Table 1 Summary of scanning transmission electron microscopy (STEM) data used for label distribution analyses. STEM images were collected in 3 different experiments to compare the distribution of quantum dot (QD)-labels by pair correlation analysis. Data sets comprised STEM images acquired at actin-rich (n=3), actin-low regions (n=3) and Cytochalasin D (CD) treated (n=2) SKBR3 breast cancer cells that were transduced with actin-green fluorescent protein (GFP).

Data Set	Number of QD-labels	Number of Chains (≥ 6 QD-labels)	Density of Chains	Number of Chains in simulated data	N (Random Data)	p-Value
1	599	1	0.24/µm²	1	100×	<0.02
2	1,030	1	0.24/µm²	1×1; 2×2	100×	<0.04
3	1,430	12	2.87/µm²	4×2; 3×1	100×	<0.01

Table 2. Comparison of experimental -, and simulated random data of linear QD-chains. Linear chains of QD-labels of ≥ 6 QD-labels with an inter-label distance of 36 ±15 nm and angle of 180±30° were detected in STEM images. For each experimental data set, 100 randomly simulated data sets were generated with the same particle density as found in the experimental data. Number of chains in simulated data gives the number of randomly

simulated data sets in which 1 or 2 chains per image were found. The probability of finding at least the same number of chains detected in the experimental data in the simulated data is listed in the last column. A p-valued <0.05 was considered significant.

Schemes

Scheme 1. Pseudo-code for detection of linear QD chains.

Algorithm Linear Particle Chain Finder

Input particle positions $p_1,\ldots,p_N$

begin

1: compute distance matrix $D \in R^{N\times N}$

($d_{ij} \in D$ Contains the distance from particle p_i to p_j)

2: construct adjacency matrix $A \in R^{N\times N}$, where

$$a_{ij} := \begin{cases} 1 & if\ d_{ij} \in [21,51] \\ 0 & else \end{cases}$$

(Corresponds to 36±15 nm particle distance)

3: Solve graph problem "find all paths l of length $k = 6$ from p_i to p_j" on A using Yen's algorithm.[49] Results in paths $l \in L$.

4: For each l compute Pearson product-moment correlation coefficient c.[50] If $c < 0.9$, discard l.

5: For each two consecutive line segments of each path l compute the enclosing angle α. If $\alpha > 30°$, discard l.

end

Output set L of linear particle chains (can be empty)

Figure Captions

Figure 1. Schematics of whole cell analysis of membrane proteins.

I. Transduction of SKBR3 cells, seeded on silicon microchips with a silicon nitride membrane, with actin- reen fluorescent protein (GFP)-constructs and cultivation of cells for 40h. **II.** Optional treatment with 2µM Cytochalasin D for 1h at 37°C for actin-breakdown-experiments. **III.** Labeling of ErbB2 with specific Affibody-biotin-conjugates against extracellular part of ErbB2 (1:1 binding stoichiometry). After fixation, the samples were incubated with Streptavidin-coupled quantum dots (QDs) and prospected to fluorescence microscopy (FM) (**IV.**). After post-fixation, the samples were covered with graphene films and examined by scanning transmission electron microscopy (STEM).

Figure 2. Correlative FM and STEM of whole breast cancer cells. (a, c) Cropped fluorescence micrographs of SKBR3 breast cancer cells showing cellular actin-GFP in green (λ_{max}=520 nm) and QD-labeled membrane ErbB2 in red (λ_{max}=655 nm). Areas were both signals overlay appear yellow. Actin containing ruffles can be identified as bright green and yellowish lines at the cell edges. (b, d) Corresponding STEM micrographs of graphene covered breast cancer cells acquired at the same spots, b: 1000×, d: 4,000×. (e, f) High resolution STEM micrographs of regions marked in c, d. QD-labels appear as white dots and membrane ruffles in (e) in a light grey tone when compared to flat cell regions in (f), e: 100,000×, f: 120,000×.

Figure 3. Graphs of pair correlation functions *g*(*r*) as the function of the radial distance *r* between QD-labels collected at actin-rich (a) and actin-low (b) cell regions. (a) *g*(*r*) (blue) of QD-label distances collected in 27 images (n=3) of actin-rich cell regions. Arrowhead

marks peak at 20 nm. $g(r)$ (grey) of simulated data of labels from 27 randomly generated images with the same particle density as found in actin-rich regions (s. table 1). (b) $g(r)$ (black) of QD-label distances collected in 17 images (n=3) of actin-low cell regions. Arrow marks peak at 36 nm. $g(r)$ (grey) of simulated data of labels from 17 randomly generated images with the same particle density as found in actin-low regions (see Table 1).

Figure 4. STEM of whole breast cancer cells treated with Cytochalasin D (CD). (a) STEM of graphene covered SKBR3 breast cancer cells (30,000×), (b) STEM image of region marked in a (100,000×). Automatically detected QD-labels are marked in yellow to enhance visibility. (c) $g(r)$ (green) of radial QD-label distances collected in 7 images (n=2) of cell edges of CD treated cells. Black arrow marks peak at 36 nm. $g(r)$ (grey) of simulated data of labels from 7 randomly generated images with the same particle density as found in average in imaged regions of CD treated breast cancer cells (s. table 1).

Figure 5. Correlative FM and STEM of QD-labeled ErbB2 on whole breast cancer cells revealing linear QD-chains in actin rich region. (a) Cropped fluorescence micrographs of SKBR3 breast cancer cells showing cellular actin-GFP in green (λ_{max}=520 nm) and QD-labeled membrane ErbB2 in red (λ_{max}=655 nm). Areas were both signals overlay appear yellow. (b) Corresponding scanning transmission electron micrographs of graphene covered breast cancer cells taken at the same spot (1000×). (c) STEM micrograph of region marked in a, b at 30,000×. Note that actin containing regions appear in a light grey tone (e) when compared to flat cell regions (d). (d, e) STEM micrographs of regions marked in c at 100,000 × magnification. Automatically detected QD-labels are marked in yellow to enhance visibility. In e the white dotted line marks a linear QD-chain consisting of 6 QD-labels with an inter-label distance of 36 ±15 nm and angle of 180±30°.

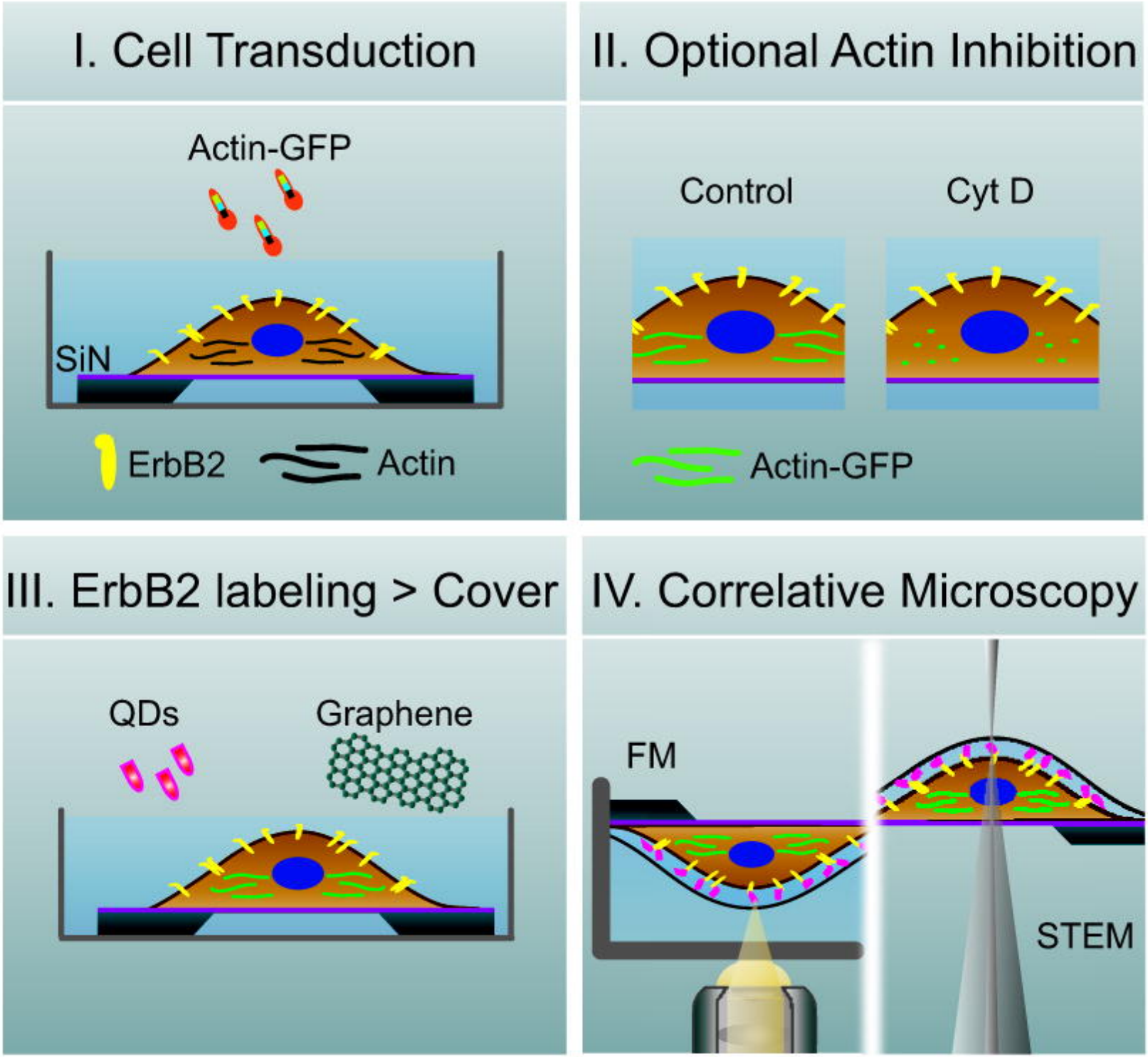
I. Cell Transduction
Actin-GFP
SiN
ErbB2
Actin
II. Optional Actin Inhibition
Control
Cyt D
Actin-GFP
III. ErbB2 labeling > Cover
QDs
Graphene
IV. Correlative Microscopy
FM
STEM

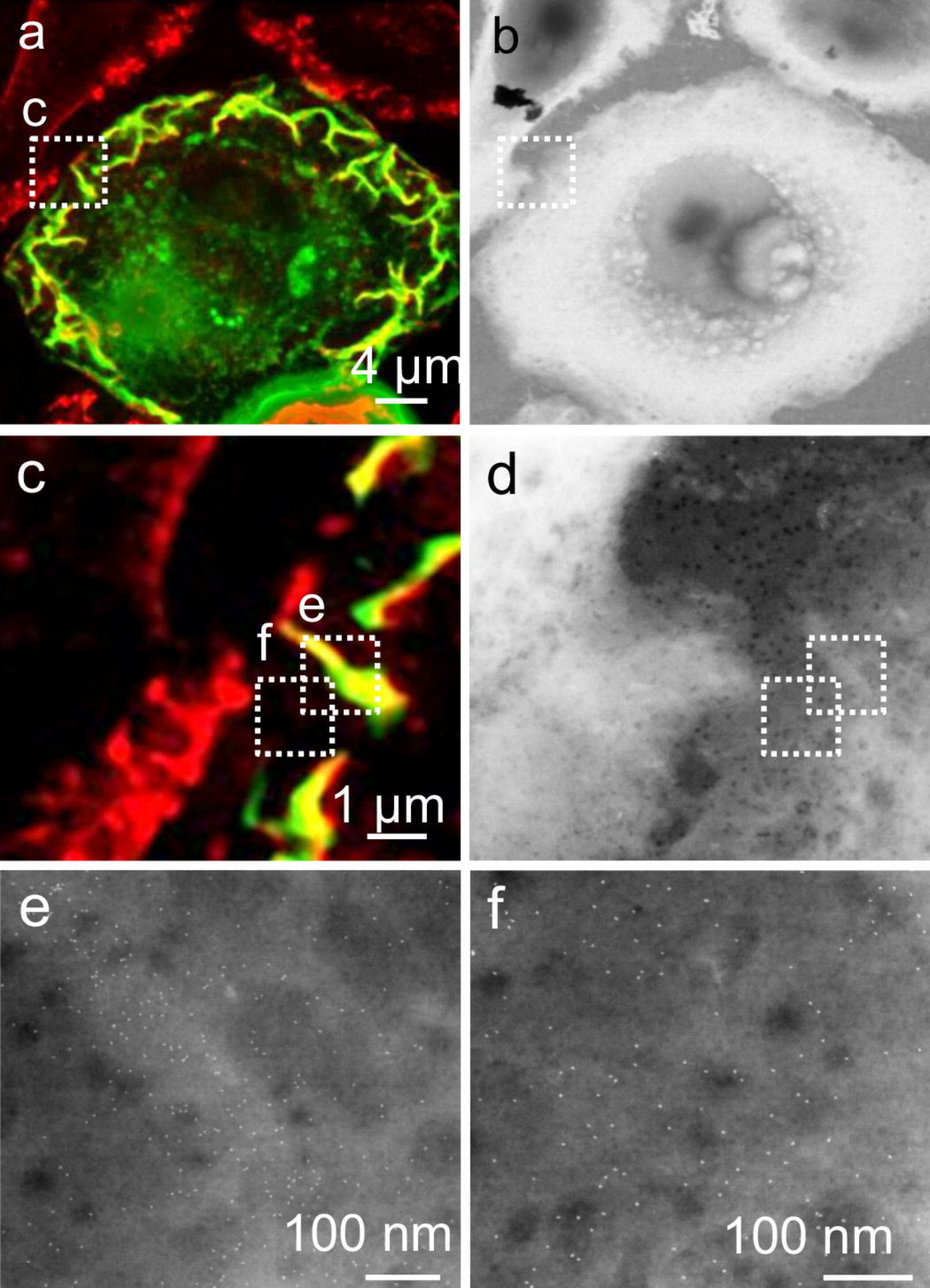
a
c
4 µm
b
c
e
f
1 µm
d
e
100 nm
f
100 nm

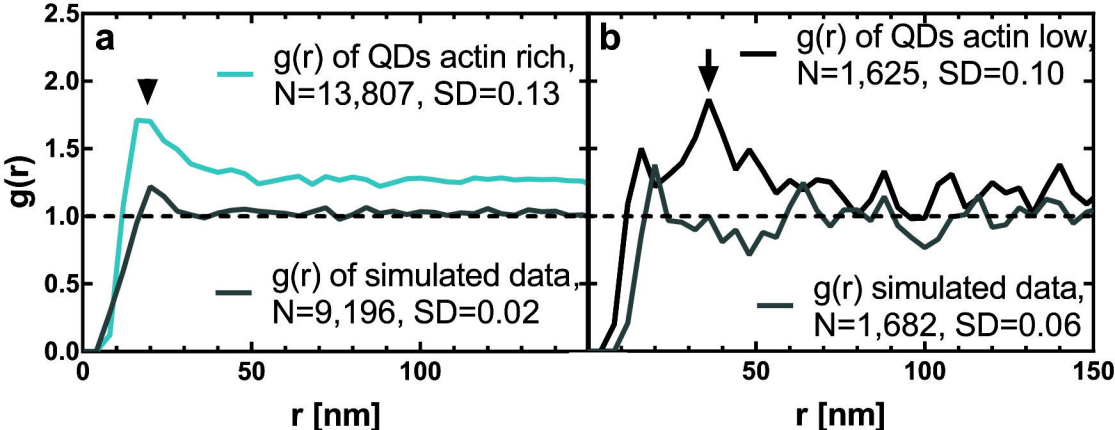
a
g(r) of QDs actin rich,
N=13,807, SD=0.13
g(r) of simulated data,
N=9,196, SD=0.02
b
g(r) of QDs actin low,
N=1,625, SD=0.10
g(r) simulated data,
N=1,682, SD=0.06
g(r)
r [nm]
r [nm]
0.0
0.5
1.0
1.5
2.0
2.5
0
50
100
50
100
150

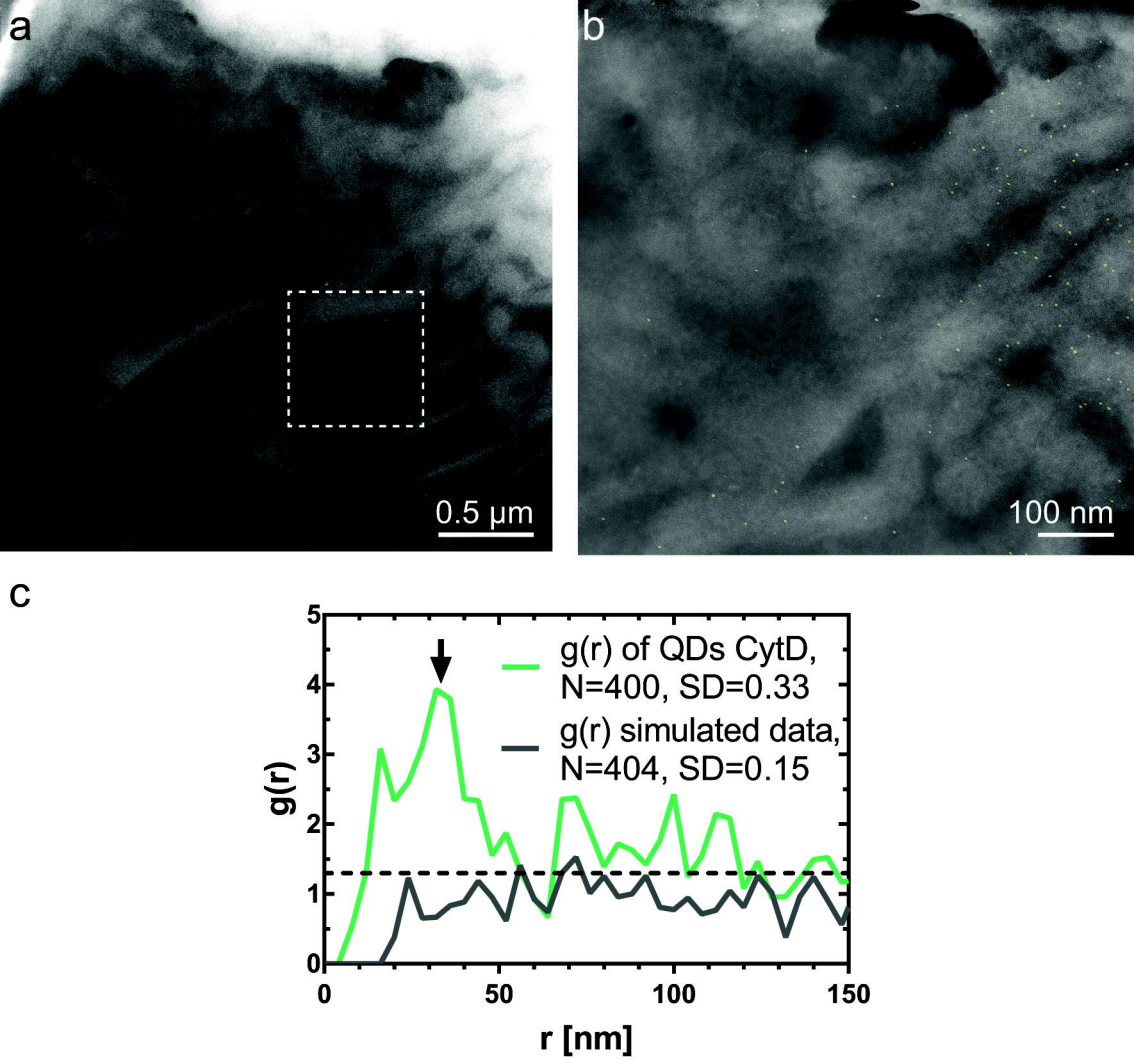
a
0.5 µm
b
100 nm
c
g(r) of QDs CytD,
N=400, SD=0.33
g(r) simulated data,
N=404, SD=0.15
g(r)
r [nm]
0
1
2
3
4
5
0
50
100
150

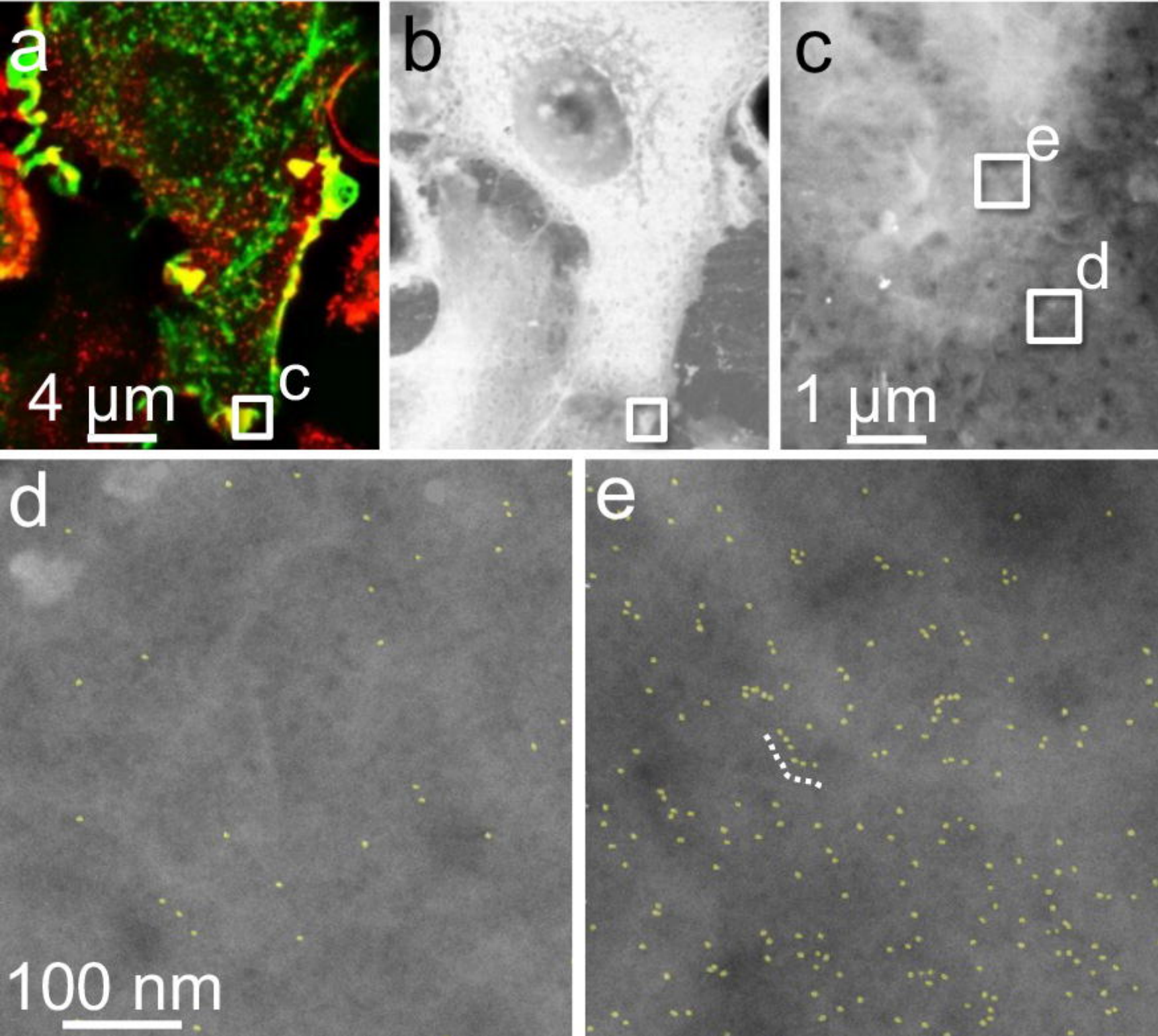
a
4 µm
c
b
c
e
d
1 µm
d
100 nm
e